



Discover Generics

Cost-Effective CT & MRI Contrast Agents

 **FRESENIUS
KABI**

[WATCH VIDEO](#)

AJNR

Tuberculous arachnoiditis of the spine: findings on myelography, CT, and MR imaging.

K H Chang, M H Han, Y W Choi, I O Kim, M C Han and C W Kim

AJNR Am J Neuroradiol 1989, 10 (6) 1255-1262
<http://www.ajnr.org/content/10/6/1255>

This information is current as of June 23, 2025.

Tuberculous Arachnoiditis of the Spine: Findings on Myelography, CT, and MR Imaging

Kee Hyun Chang¹
 Moon Hee Han
 Yo Won Choi
 In One Kim
 Man Chung Hari
 Chu-Wan Kim

Tuberculosis (TB) is a rare cause of spinal arachnoiditis. It may occur primarily or secondary to intracranial or vertebral infection; unlike other types of arachnoiditis, it frequently involves the spinal cord as well as the meninges and the nerve roots. We retrospectively reviewed 13 conventional myelograms, eight CT myelograms, and five Gd-DTPA-enhanced MR images in 13 patients with spinal TB radiculomyelitis (arachnoiditis). Eleven patients had intracranial TB meningitis at the time of diagnosis or before. Ten patients were less than 30 years old. Conventional myelographic findings included a block of the CSF (11/13), most commonly at the level of the conus medullaris; irregular or indistinct thecal sac contour (9/13); multiple fine and/or coarse nodular defects (8/13); nerve-root thickening (7/13); and vertical bandlike adhesive defects (4/13). CT myelography showed intradural nodular masses suggesting tuberculomas at or just above the level of the block (4/8), irregularity of the spinal cord surface (4/8), irregular filling or obliteration of subarachnoid space (6/8), and root thickening (5/8). Gd-DTPA-enhanced MR images revealed enhancing nodules suggesting tuberculomas (2/5); enhancement of the dura-arachnoid complex around the cord (3/5); and segmental enhancement of the thoracic cord, suggesting either infarction caused by vasculitis or TB myelitis in association with diffuse cord swelling (1/5). Plain MR findings were much less conspicuous, showing only an indistinct or irregular dura-arachnoid-cord complex (4/5).

In conclusion, the conventional myelographic findings are considered to be virtually diagnostic of spinal TB radiculomyelitis in young patients with antecedent or coexisting TB meningitis. CT myelography and Gd-DTPA-enhanced MR imaging seem to be useful adjunctive methods, especially in patients in whom spinal subarachnoid blocks are seen on conventional myelography.

AJNR 10:1255-1262, November/December 1989

Among the various causes of spinal arachnoiditis, the tuberculous (TB) infection has remained an important clinical problem in some less developed countries, although it appears to be very rare in the advanced countries of the Western world [1, 2]. Unlike the more common noninfectious lumbosacral arachnoiditis [3-5], the spinal intradural TB infection frequently involves the spinal cord as well as the meninges and nerve roots [1, 6-8]. Wadia and Dastur [9, 10] suggested that the designation TB radiculomyelitis be applied to cases previously categorized as arachnoiditis, intradural spinal tuberculoma, granuloma, or spinal cord complications of TB meningitis. The diagnosis of spinal TB radiculomyelitis can be suspected on the basis of a history of intracranial TB meningitis, clinical manifestations, and CSF laboratory data. The microorganism is rarely identified from analysis of CSF [1, 2, 6-10]. In practice, the radiologic findings often play a critical role in the diagnosis and management of this disease. To our knowledge, there have been few descriptions of the radiologic features of spinal TB radiculomyelitis [3, 8, 10]. The purpose of this article is to describe the myelographic, CT, and MR findings of spinal TB radiculomyelitis in detail.

Received February 3, 1989; revision requested April 5, 1989; revision received May 2, 1989; accepted May 4, 1989.

This work was supported in part by a grant from the clinical research fund of Seoul National University Hospital (1988).

¹ All authors: Department of Radiology, College of Medicine, Seoul National University, Seoul, Korea. Address reprint requests to K. H. Chang, Department of Diagnostic Radiology, Seoul National University Hospital, 28, Yeongun-Dong, Chongro-Ku, Seoul 110-744, Korea.

0195-6108/89/1006-1255
 © American Society of Neuroradiology

TABLE 1: Summary of Clinical and Radiologic Features in Patients with Spinal Tuberculous (TB) Radiculomyelitis

Case No.	Age	Gender	History/Major Clinical Features	Conventional Myelography	CT Myelography	Spinal MR	Brain CT
1 ^a	22	F	Intracranial TB meningitis 2 years before; paraparesis for 1 year	Complete block at level of conus medullaris; multiple fine nodular defects; localized root thickening	Nodular mass adherent to posterior surface of cord, showing pear-shaped cord; localized root thickening	Not performed	Not performed
2 ^b	29	F	Coexisting intracranial TB meningitis; headache, voiding difficulty for 2 months	Complete block at level of conus medullaris; localized root thickening; irregular vertical bandlike defect; irregular thecal sac contour	Nodular mass adherent to posterior surface of cord; localized root thickening; irregular filling of subarachnoid space; irregular cord surface	Not performed	Communicating hydrocephalus with basal cisternal enhancement and granulomas
3	43	M	Intracranial TB meningitis 27 years before; paraparesis for 13 years	Multiple fine nodular defects; vertical bandlike defect	Not performed	Not performed	Not performed
4	29	F	Coexisting intracranial TB meningitis; paraparesis for 2 months	Incomplete block at T7 level; multiple fine and coarse nodular defects; localized root thickening	Not performed	Not performed	Communicating hydrocephalus with basal cisternal enhancement
5	6	M	Intracranial TB meningitis 1 year before; paraparesis for 4 months	Complete block at level of conus medullaris; multiple fine nodular defects	Not performed	Not performed	Communicating hydrocephalus
6 ^a	37	M	Low back pain, jerky movement of both lower limbs for 7 years; urinary incontinence for 7 months	Complete block at T9 level on C1-C2 puncture (dry tap on lumbar puncture); irregular thecal sac contour	Nodular mass adherent to posterior surface of cord; irregular filling of subarachnoid space	Not performed	Communicating hydrocephalus
7 ^b	22	F	Coexisting intracranial TB meningitis; headache, gait disturbance for 2 months	Incomplete block at T7 level; diffuse root thickening; irregular thecal sac contour	Partial obliteration of subarachnoid space; diffuse root thickening	Not performed	Communicating hydrocephalus with basal cisternal enhancement
8	29	F	Coexisting intracranial TB meningitis; paraparesis, voiding difficulty for 1 month	Incomplete block at level of conus medullaris; multiple fine and coarse nodular defects; localized root thickening; irregular thecal sac contour	Not performed	Not performed	Communicating hydrocephalus with basal cisternal enhancement and granulomas
9 ^b	14	F	Coexisting intracranial TB meningitis; paraplegia and paresthesia of bilateral lower limbs for 3 weeks	Complete block at T10 level; multiple fine and coarse nodular defects; vertical bandlike defect; irregular thecal sac contour	Irregular filling of subarachnoid space; irregular cord surface	Diffuse edematous cord swelling; segmental enhancement of cord at T4-T6 level; intradural focal nodular enhancement at T9, T11 levels; indistinctness between dura, subarachnoid space, and cord; enhancement of dura-arachnoid complex around cord	Communicating hydrocephalus with basal cisternal enhancement

Table 1 continues

TABLE 1—Continued

Case No.	Age	Gender	History/Major Clinical Features	Conventional Myelography	CT Myelography	Spinal MR	Brain CT
10 ^a	20	F	Intracranial TB meningitis 3 months before; headache, paraparesis, hypesthesia of bilateral lower limbs for 1 month	Incomplete block at level of conus medullaris; multiple fine nodular defects; vertical bandlike defect; localized root thickening; irregular thecal sac contour	Nodular mass adherent to posterior surface of cord; localized root thickening; irregular cord surface	Intradural ringlike enhancing nodules posterior to cord at T11–T12 level; enhancement of dura-arachnoid complex around cord	Communicating hydrocephalus
11	24	M	Intracranial TB meningitis 20 years before; back pain, progressive paraparesis for 3 years	Indistinct thecal sac contour	Not performed	Indistinctness between dura, subarachnoid space, and cord; marginal irregularity of dura-arachnoid-cord complex	Suprasellar calcifications, ventriculo-peritoneal shunt
12	65	F	Coexisting TB spondylitis at C7–T2; neck stiffness, paraparesis, urinary incontinence for 2 weeks	Incomplete block at T5 level; indistinct thecal sac contour at T1–T5 levels; apparent rootless thecal sac showing "empty sac" in lumbar level	Intraspinal epidural plaque-like mass associated with vertebral destruction at C7–T2 level; partial obliteration of subarachnoid space on left at T1–T5 level; peripheral arrangement of roots with adhesion to dura in lumbar area	Indistinctness between dura, subarachnoid space, and cord; vertebral destruction of C7–T2, disk-space narrowing, plaque-like enhancing retrovertebral mass compressing dural sac	Normal
13	16	F	Coexisting intracranial TB meningitis; paraparesis, paresthesia of bilateral lower limbs, urinary difficulty for 3 months	Complete block at T10 level; multiple fine and coarse nodular defects; localized root thickening; irregular thecal sac contour	Irregular filling of subarachnoid space; localized root thickening; irregular cord surface	Indistinctness between dura, subarachnoid space, and cord; enhancement of dura-arachnoid complex around cord	Communicating hydrocephalus with basal cisternal enhancement and granulomas

^a Surgically proved cases.

^b Acid-fast bacilli were found in the CSF.

Materials and Methods

We retrospectively reviewed 13 conventional myelograms, eight CT myelograms, and five MR examinations from 13 consecutive patients with spinal TB radiculomyelitis studied in the past 4 years. The four male and nine female patients were 6–65 years old (average age, 27.3 years). The diagnosis was established on the basis of clinical history and manifestations, laboratory findings in the CSF, and myelographic findings in all patients. Acid-fast bacilli were isolated from the CSF in four patients, and pathologic proof was obtained through spinal surgery in two other patients. Eleven patients had intracranial TB meningitis at the time of or before the diagnosis. One had coexisting TB spondylitis. The clinical symptoms varied, but the most common one was paraparesis of variable duration. The CSF data showed active inflammatory findings (lymphocytosis, elevated protein, and decreased glucose) in eight patients (six with active intracranial meningitis and one each with communicating hydrocephalus and TB spondylitis), elevated CSF protein in three, and normal CSF findings in two. There was a gradual or rapid response to antituberculous drugs in all except two patients (cases 3 and 11). Brain CT scans were obtained within 1 month of myelography in 11

patients. The findings consisted of active TB meningitis with basal cisternal enhancement (six), communicating hydrocephalus without cisternal enhancement (three), suprasellar calcification caused by old TB meningitis (one), and normal findings (one). Lumbar puncture had been performed in 11 patients with previous or coexisting intracranial meningitis, but none had a history of spinal surgery or intrathecal injection of drugs. Plain radiographs of the chest showed TB lesions in five patients. Myelography was performed with instillation of 7–8 ml of metrizamide (Amipaque, Winthrop) in a 180 mg/ml concentration or iopamidol (Niopam 300, Bracco) in a 300 mg/ml concentration through the lumbar route in 12 patients and through the cervical route in one patient, because of a dry tap on lumbar puncture. Spinal CT scans were obtained immediately after myelography in eight patients. The CT section was through the level of CSF block and included several centimeters above and below that level. The section thickness was 1 cm. In five patients, MR images were obtained with a superconducting system operating at 2.0 T.* With a rectangular surface coil, all images were produced by using multislice, multiecho, spin-

* Spectro-20000, Goldstar, Seoul, Korea.

echo (SE) sequences. After nonenhanced T1-weighted, 500/30 (TR/TE), intermediate-weighted, 3000/30, and T2-weighted, 3000/80, images were obtained in the sagittal plane, Gd-DTPA- (0.1 mmol/kg body weight) enhanced T1-weighted images were obtained in the sagittal and axial planes. Slice thickness/gap was 3 mm/1 mm in the sagittal plane and 5 mm/1 mm in the axial plane.

Results

The clinical and radiologic features of the 13 patients are summarized in Table 1.

The most common conventional myelographic finding was a block of the CSF, which was seen in 11 patients (complete block in six and incomplete block in five) (Figs. 1–3). The block was seen at the level of the conus medullaris in five, at

T7 in two, at T9–T10 in three, and at T5 in one. The margin of the block appeared to have an irregular outline. The second common finding was the localized or diffuse irregularity or indistinctness of the thecal sac contour, which was seen in nine patients (Figs. 2 and 3). The third common finding was that of multiple nodular defects; this was observed in eight patients. There were two types of nodular defects: one type, multiple, fine, uniform-sized nodular defects as small as 1–2 mm, was seen in four patients (Fig. 1); the other type, several coarse, nodular defects ranging in size from 3 to 10 mm, was seen in association with fine nodular defects in the other four patients (Figs. 3 and 4). The nodular defects were somewhat irregular and fuzzy in outline and were scattered throughout the entire lumbar level. The other conspicuous findings were nerve-root thickening (Figs. 1, 2, and 4) and vertical, bandlike

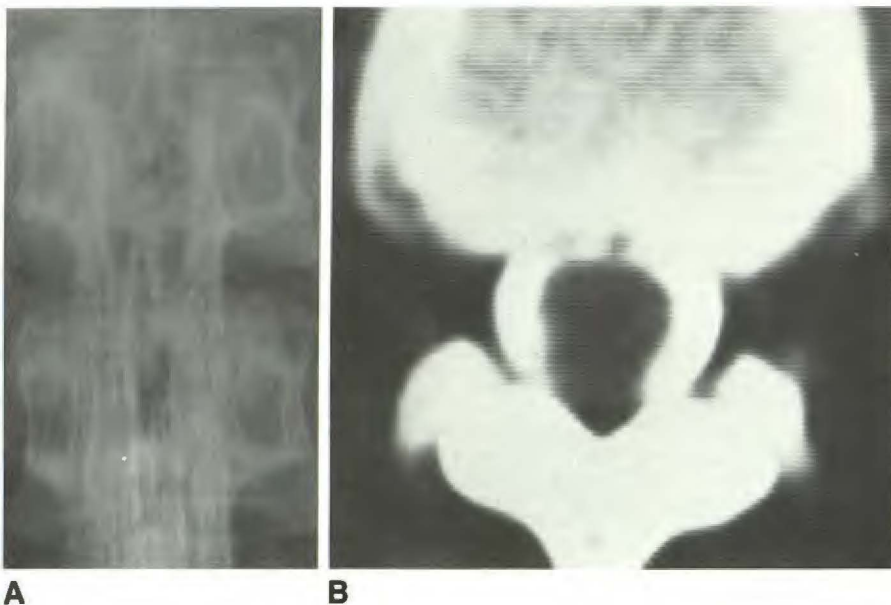


Fig. 1.—Case 1.

A, Conventional myelogram reveals complete block at lower thoracic level, multiple fine nodular defects, and localized root thickening at upper lumbar level.

B, CT myelogram at conus level shows apparent pear-shaped cord caused by round mass tightly adhered to posterior surface of cord, suggesting tuberculoma, which was surgically confirmed.

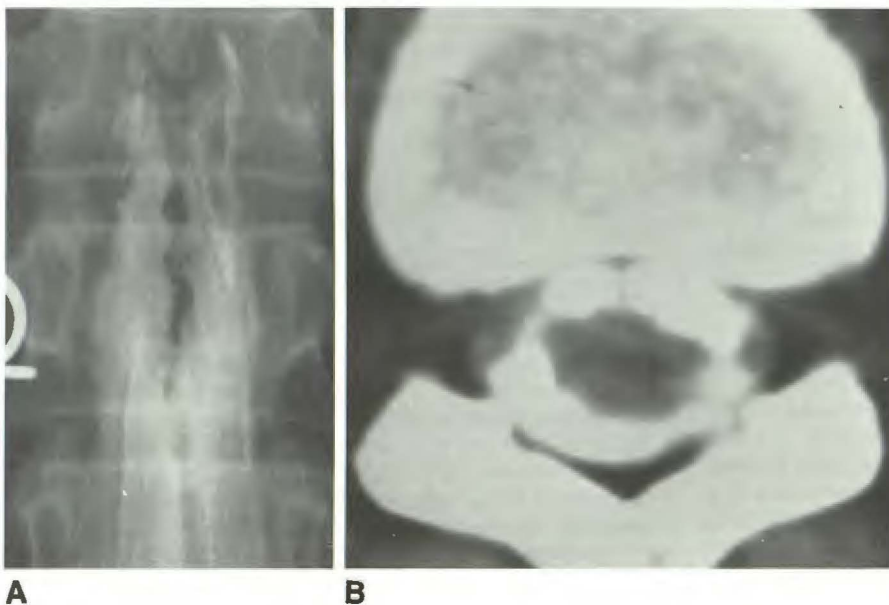


Fig. 2.—Case 2.

A, Conventional myelogram reveals complete block at level of conus medullaris, irregularity of thecal sac contour, root thickening, and irregular vertical bandlike defect.

B, CT myelogram at lower thoracic level shows irregular surface of spinal cord and irregular filling of subarachnoid space.

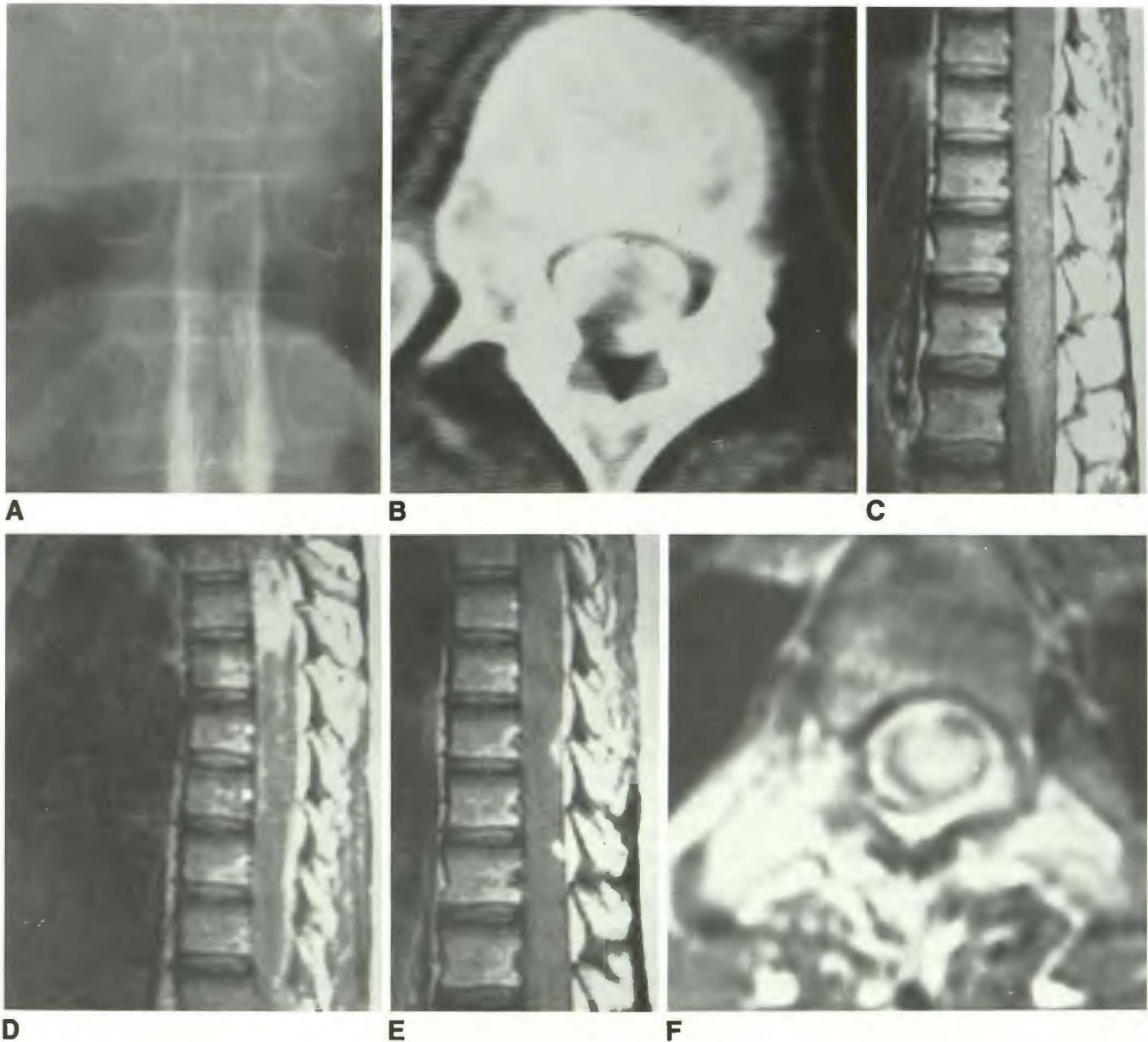


Fig. 3.—Case 9.

A, Conventional myelogram shows complete block at T10 level, multiple fine and coarse nodular defects, a vertical bandlike defect, and irregularity of thecal sac margin.

B, CT myelogram at T10–T11 level shows irregular filling of subarachnoid space.

C, Nonenhanced sagittal SE 500/30 image reveals apparently diffuse enlargement of thoracic cord with no distinction between cord, subarachnoid space, and meninges.

D and E, Gd-DTPA-enhanced sagittal SE 500/30 images reveal segmental enhancement of cord at T4–T6 level, smaller focal nodular enhancement at posterior portion of dural sac at T9 and T11 levels, and plaquelike enhancement of meninges.

F, Gd-DTPA-enhanced axial SE 500/30 image through T5 level. Dura-arachnoid complex and spinal cord are densely enhanced, suggesting either infarction or tuberculous myelitis.

defects (Figs. 2 and 3); these were demonstrated in seven and four patients, respectively. The root thickening was localized in five patients.

The CT myelogram showed an irregular or smooth nodular mass adherent to the dorsal surface of the spinal cord at or just above the block in four of eight patients; some cords appeared pear-shaped (Fig. 1). Thickening of the nerve roots

was demonstrated at the upper lumbar levels in five patients. Irregular filling or partial obliteration of the subarachnoid space was found around the level of the block in six patients (Figs. 2 and 3). In four patients, the spinal cord around the level of the block appeared to have an irregular surface (Fig. 2).

Gd-DTPA-enhanced T1-weighted MR images revealed enhancing nodules in the posterior portion of the thecal sac at

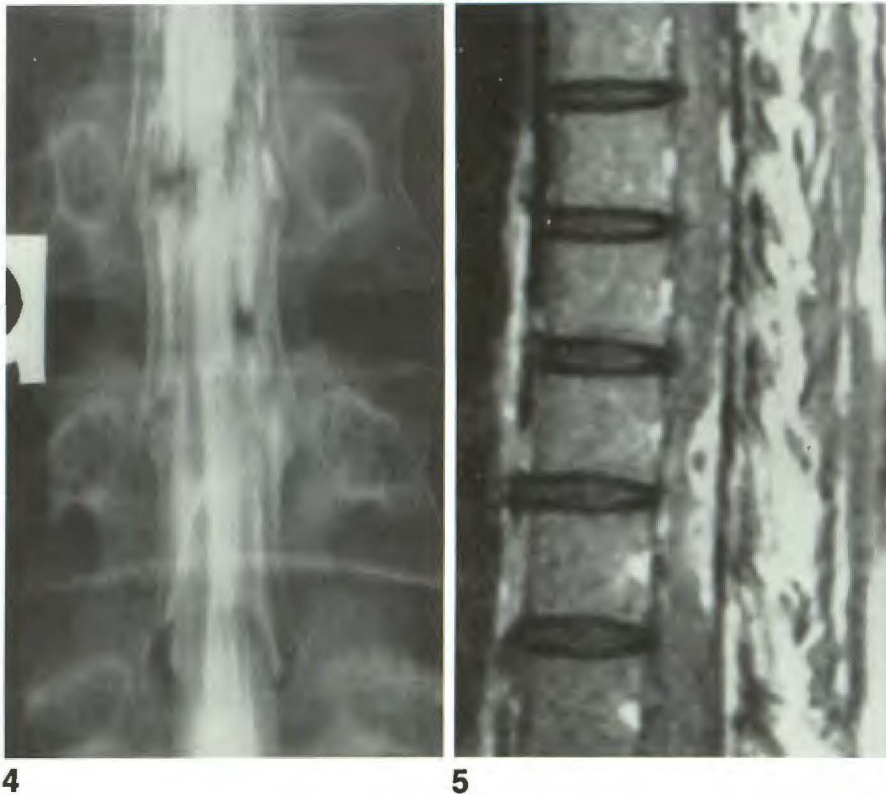


Fig. 4.—Case 4. Conventional myelogram shows multiple coarse and fine nodular defects and localized root thickening. Nodular defects do not appear round, but rather have an irregular and fuzzy outline.

Fig. 5.—Case 10. Gd-DTPA-enhanced sagittal SE 500/30 image reveals multiple ringlike enhancing nodules suggesting tuberculomas in posterior portion of dural sac at T11-T12 level and plaque-like enhancement of dura-arachnoid complex.

the lower thoracic levels in two of five patients; in one, the enhancement was ringlike (Fig. 5). The diffuse or localized enhancement of the dura-arachnoid complex around the cord was seen in three patients (Figs. 3, 5, and 6). In one (case 9), there was segmental enhancement of the cord itself at the T4-T6 level in association with diffuse swelling of the cord (Fig. 3). On plain MR images, the spinal cord appeared to be indistinguishable from the subarachnoid space and the dura in four cases, and the dura-arachnoid-cord complex appeared to have an irregular outline in one case.

Discussion

There is unanimous agreement that spinal TB radiculomyelitis is a secondary TB lesion, although it may rarely occur primarily [6]. Wadia [10] suggested a classification based on the site of origin: (1) primary TB spinal radiculomyelitis, (2) radiculomyelitis secondary to TB basal meningitis, and (3) radiculomyelitis secondary to vertebral TB. In our series, 85% (11/13) of cases were secondary to intracranial TB meningitis and 8% (1/13) were secondary to vertebral infection. Secondary radiculomyelitis may appear during the acute stage of the primary lesion or in variable periods after the onset of disease [1, 8]. Kozlowski [8] described two cases of adhesive arachnoiditis developing 7 and 9 years after intracranial TB meningitis. In two patients in our series, spinal manifestations were seen after a lapse of 14 and 17 years (cases 3 and 11, respectively).

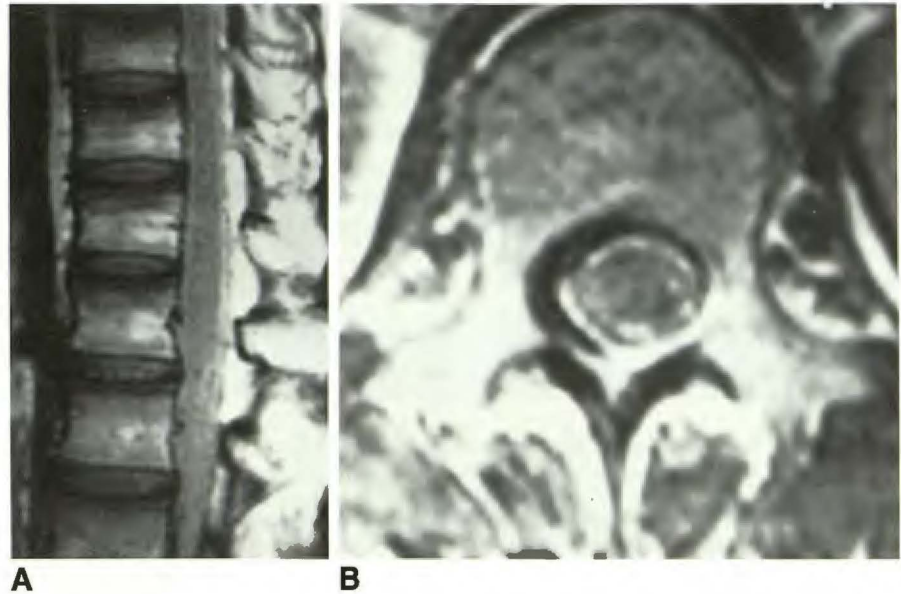
Although the prevalence of the typical form of spinal arach-

noiditis remains highest in the 30-50-year age group [3], spinal TB radiculomyelitis occurs almost exclusively in patients less than 30 years old [6]. In our series 77% (10/13) were younger than 30 years old. Clinical features of spinal TB radiculomyelitis are varied and include paraplegia, quadriplegia, pain, and other root symptoms, depending on the sites involved [1, 2, 6-10]. In our series 77% of patients had paraparesis or paraplegia.

In the early stage of spinal TB radiculomyelitis, whether the lesion is primary or secondary, the meninges of the cord may show a variable degree of congestion and inflammatory exudate throughout their course. The spinal cord and nerve roots may be surrounded by gelatinous exudate and be edematous. The tuberculoma, or TB abscess, may be associated anywhere within the thecal sac. It is usually closely adherent to the inner aspect of the dura mater and to the spinal cord into which it digs a crater, so that occasionally it is difficult to determine whether the intradural tuberculoma is extramedullary or intramedullary, emerging to the surface after having broken through the spinal cord [6, 8]. Arseni and Samitca [6] reported eight cases of intradural TB granulomas, three of which were intradural extramedullary and five intramedullary. In the chronic stage, the fibrin-covered roots stick to each other as well as to the thecal sac. Eventually, dense collagenous adhesions are formed by proliferating fibrocytes during the repair process.

All the radiologic features reflect the pathologic process described above. In our series, the spinal subarachnoid block on conventional myelography was believed to have been

Fig. 6.—Case 13.
A and B, Gd-DTPA-enhanced T1-weighted sagittal (A) and axial (B) SE 500/30 images show diffuse enhancement of dura-arachnoid complex around cord.



caused by tuberculomas, arachnoid adhesions, and/or cord swelling. The block of the CSF in TB radiculomyelitis has a distinct preference for the thoracic segment of the spine [6, 8], as was seen in our series. The exact cause of the block could not be evaluated with conventional myelography alone. CT and MR imaging, however, delineated the intrathecal pathologic state more precisely, particularly at the level above the block, showing masses suggesting tuberculomas at or above the level of the block. Multiple fine or coarse nodular defects seen on conventional myelography may represent active tuberculomas or inactive scar tissue. The adhesive scar tissue appears to be more irregular in outline, but the differentiation between these two conditions may be possible only with IV contrast-enhanced CT or Gd-DTPA-enhanced MR imaging, which also demonstrated enhancement of the dura-arachnoid complex, indicating the presence of active meningeal inflammation around the cord, as seen in Figures 3, 5, and 6. Gd-DTPA-enhanced MR imaging seems to be superior to IV contrast-enhanced CT because of direct sagittal imaging and more sensitive contrast enhancement. In addition, MR imaging has the capability of demonstrating other abnormalities of the spinal cord, such as edema, ischemia/infarct, inflammation, and multiple sclerosis [11]. In case 9 (Fig. 3), the edematous swelling and segmental enhancement of the cord suggesting infarction resulting from vasculitis or myelitis could hardly be expected to be seen on CT. However, plain MR imaging appears insensitive to the detection of active inflammation of the meninges and tuberculomas, like those in intracranial meningitis and meningeal carcinomatosis [12, 13].

The nerve-root thickening reflects either the edematous swelling during the acute stage or interroot adhesion in the chronic stage. Other findings such as vertical, bandlike defects; irregular margin of the thecal sac; irregular filling or partial obliteration of the subarachnoid space; and irregular cord outline are believed to be due to the presence of scar

tissue and adhesions between nerve roots, meninges, and the spinal cord surface. Most of these features are best demonstrated on the conventional myelogram. CT myelograms and MR images provided little additional information about a chronic adhesive process without active inflammation. The role of MR imaging in the evaluation of spinal TB radiculomyelitis has not been determined as yet. Little experience with MR imaging in the study of nonspecific adhesive arachnoiditis has been reported [14–16]. Currently, conventional and CT myelography appear to be more sensitive in the detection of adhesive arachnoiditis [15], although Ross et al. [14] reported an excellent correlation between MR imaging and conventional and CT myelography in the study of nonspecific lumbar arachnoiditis. This may also apply to the study of chronic adhesive TB arachnoiditis. In our series, chronic adhesive changes were not conspicuous on either plain or Gd-DTPA-enhanced MR imaging.

The conventional myelographic appearances need to be differentiated from a number of other conditions, such as other kinds of radiculomyelitis or arachnoiditis, neurofibromas, hypertrophic interstitial polyneuritis, spinal arteriovenous malformation, and seeding from intracranial tumors and leptomeningeal carcinomatosis, including lymphoma [17–22]. The greatest difficulty is the differentiation from leptomeningeal carcinomatosis. Leptomeningeal carcinomatosis can produce CSF block, multiple nodular defects, nerve-root thickening, and/or adhesion of nerve roots, characteristics shared by TB radiculomyelitis [18, 19]. However, in TB radiculomyelitis the nodular defects appear to have an irregular and fuzzy outline, the root thickening is more localized, and the adhesive vertical bandlike defects are frequently associated; in meningeal carcinomatosis the nodular defects appear to have a discrete and sharp margin, the root thickening is more diffuse and uniform, and the adhesive vertical bandlike defects are not usually associated [18–22]. In practice, a combination of the above myelographic findings in young patients with antecede-

ent or coexisting TB meningitis is virtually diagnostic of TB radiculomyelitis. Both CT myelography and Gd-DTPA-enhanced MR imaging appear to be useful adjuncts to conventional myelography, especially in patients with spinal blocks on conventional myelography.

In conclusion, conventional myelography remains the primary radiologic method for diagnosing suspected spinal TB radiculomyelitis, particularly in patients with chronic adhesive changes. However, in patients suspected of having an active inflammatory process within the thecal sac or myelopathy, Gd-DTPA-enhanced MR imaging may be the optimal primary imaging technique, obviating invasive myelography.

REFERENCES

- Freilich D, Swash M. Diagnosis and management of the paraplegia with special reference to tuberculous radiculomyelitis. *J Neurol Neurosurg Psychiatry* 1979;42:12-18
- Sheller JR, DesPrez RM. CNS tuberculosis. *Neurol Clin* 1986;4:143-158
- Shaw MDM, Russel JA, Grossart KW. The changing pattern of spinal arachnoiditis. *J Neurol Neurosurg Psychiatry* 1978;41:97-107
- Jorgensen J, Hansen PH, Steenkov V, Qvesen N. A clinical and radiological study of chronic lower spinal arachnoiditis. *Neuroradiology* 1975;9:139-144
- Burton CV. Lumbosacral arachnoiditis. *Spine* 1978;3:24-30
- Arseni G, Samitca DC. Intraspinous tuberculous granuloma. *Brain* 1960;83:285-292
- Bucy PC, Oberhill HR. Intradural spinal granulomas. *J Neurosurg* 1950;7:1-12
- Kozlowski K. Late spinal blocks after tuberculous meningitis. *AJR* 1963;90:1220-1226
- Wadia NH, Dastur DK. Spinal meningitides with radiculomyelopathy. Part I: Clinical and radiological features. *J Neurol Sci* 1969;8:239-260
- Wadia NH. Radiculomyelopathy associated with spinal meningitides (arachnoiditis) with special reference to the spinal tuberculous variety. In: Spillane JD, ed. *Tropical neurology*. London: Oxford University, 1973: 63-72
- Haughton VM. MR imaging of the spine. *Radiology* 1988;166:297-301
- Sze G. Infections and inflammatory diseases. In: Stark DD, Bradley WG, eds. *Magnetic resonance imaging*, 1st ed. St. Louis: Mosby, 1988: 316-343
- Krol G, Sze G, Malkin M, Walker R. MR of cranial and spinal meningeal carcinomatosis: comparison with CT and myelography. *AJR* 1988;151:583-588
- Ross JS, Masaryk TJ, Modic MT, et al. MR imaging of lumbar arachnoiditis. *AJNR* 1987;8:885-892
- New PFJ, Shoukimas GM. Thoracic spine and spinal cord. In: Stark DD, Bradley WG, eds. *Magnetic resonance imaging*. St Louis: Mosby, 1988: 632-665
- Sze G. Gadolinium-DTPA in spinal disease. *Radiol Clin North Am* 1988;26:1009-1024
- Rao CVGK, Fitz CR, Harwood-Nash DC. Dejerine-Sottas syndrome in children (hypertrophic interstitial polyneuritis). *AJR* 1974;122:70-74
- Prentice WA, Kieffer SA, Gold LHA, Bjornson RGB. Myelographic characteristics of metastasis to the spinal cord and cauda equina. *AJR* 1973;118:682-689
- Guyer PB, Westbury H, Cook PL. The myelographic appearance of spinal cord metastasis. *Br J Radiol* 1968;41:615-619
- Kim KS, Ho SU, Weinberg PE, Lee C. Spinal leptomeningeal infiltration by systemic cancer: myelographic features. *AJR* 1982;139:361-365
- McAllister MD, O'Leary DH. CT myelography of subarachnoid leukemic infiltration of the lumbar thecal sac and lumbar nerve roots. *AJNR* 1987;8:568-569
- Allen MWV, Pahme ES. Lymphosarcomatous infiltration of the cauda equina. *Arch Neurol* 1962;7:476-481